Supplementary Information

Eco-Compatible Solvent-Processed High Energy Level Offset Ternary Strategy for Efficient Organic Photodetcting and Photovoltaic Applications

Min Soo Kim, Woongsik Jang, Byung Gi Kim, and Dong Hwan Wang*

School of Integrative Engineering, Chung-Ang University, 84 Heukseok-ro, Dongjak-gu, Seoul, 06974, Republic of Korea

* Corresponding author, E-mail address: king0401@cau.ac.kr (Prof. D.H. Wang)

Keywords: non-halogenated solvent; ternary; photocurrent; dark current; non-fullerene acceptor; organic electronic device

Materials

Poly(3,4-ethylenedioxythiophene):polystyrene sulfonate (PEDOT:PSS) (AI4083) as a hole transport material and 2,9-bis[3-[[3-(dimethylamino)propyl]amino]propyl]-anthra[2,1,9-def:6,5,10-d'e'f']diisoquinoline-1,3,8,10(2H,9H)-tetrone (PDINN) as an electron transport material were purchased from Heraeus and 1-Material, respectively. Poly[(2,6-(4,8-bis(5-(2-ethylhexyl-3-fluoro)thiophen-2-yl)-benzo[1,2-b:4,5-b']dithiophene))-alt-(5,5-(1',3'-di-2-thienyl-5',7'-bis(2-ethylhexyl)benzo[1',2'-c:4',5'-c']dithiophene-4,8-dione)] (PM6) as donor material and 2,2'-((2Z,2'Z)-((12,13-bis(2-butyloctyl)-3,9-diundecyl-12,13-dihydro-[1,2,5]thiadiazolo[3,4-e]thieno[2",3'':4',5']thieno[2',3':4,5]pyrrolo[3,2-g]thieno[2',3':4,5]thieno[3,2-b]indole-2,10-diyl)bis(methanylylidene))bis(5,6-difluoro-3-oxo-2,3-dihydro-1H-indene-2,1-diylidene))dimalononitrile (BTP-4F-12) as electron acceptors were purchased from Brilliant Matters. 5,5 '-[[4,4,9,9-tetrakis(2-ethylhexyl)-4,9-dihydro-s-indaceno[1,2-b:5,6-b']dithiophene-2,7-diyl]bis(2,1,3-benzothiadiazole-7,4-diylmethylidyne)]bis[3-ethyl-2-thioxo-4-thiazolidinone] (EH-IDTBR) as electron acceptor was purchased from 1-Material.

Device fabrication

The glass/ITO substrates were cleaned by sonication for 30 min with distilled water, acetone, and 2-propanol (IPA) sequentially and then blown with nitrogen gas to eliminate any residual solvent. Before spin coating the PEDOT:PSS layer onto the glass/ITO

substrate, the cleaned substrates were UV-ozone treated for 10 min for hydrophilic surface modification. The PEDOT:PSS as a hole transport layer was spin coated at 5000 rpm for 40 s and thermally treated at 140 ℃ for 10 min. The PM6:EH-IDTBR-BTP-4F-12 solution as photoactive material (at a concentration of 22 mg mL-1) was dissolved by O-xylene as the host solvent. The PM6:EH-IDTBR:BTP-4F-12 solution was spin coated onto the PEDOT:PSS-coated substrates and thermally treated at 150 ℃ for 10 min in a glove box to remove any residual solvents. Then, PDINN (1 mg mL-1 in MeOH) as an electron transporting layer was spin coated at 3000 rpm for 30 s in a glove box. Finally, an Ag cathode of thickness 100 nm was thermally evaporated onto the prepared device using a shadow mask at 4.0 × 10-6 Torr by a thermal evaporator.

Characterization

UV-visible spectroscopy (PerkinElmer Lambda 365) measurements were used to investigate the light absorption of the photoactive layer. All photovoltaic parameters were measured using the solar simulator (Peccell Tech, Inc., PEC-L01) under 1-sun illumination (AM 1.5 G 100 mW cm-2) calibrated with a silicon reference device. The J-V characteristics, SCLC, and impedance spectroscopy of the devices were measured by an electrical measurement system (ZIVE SP1). The EQE spectra were measured through a monochromator (Dongwoo Optron Co. Ltd., MonoRa-500i) after power calibration (ABET Tech, Inc., LS150). The transient photocurrent was measured by an oscilloscope (TBS2072, Tektronix, Inc., Beaverton, Oregon, United States) with a variable-gain amplifier (DLPCA-200, Femto Messtechnik Gmbh, Berlin, Germany) under customised LED illumination (LED PLC Light, Grace Lighting Int'l Co, Hong Kong). AFM images

were obtained by non-contact mode (Park NX10, Park Systems). The PL spectra of the photoactive layer was obtained using a Hitachi F-7000 fluorescence spectrophotometer at an excitation wavelength of 600 nm. The thickness images of the photoactive layer were observed by field-emission scanning electron microscopy (FE-SEM, SIGMA, Carl Zeiss, Inc.) at 5 kV. The contact angle images were measured by Phoenix-10 (SEO).

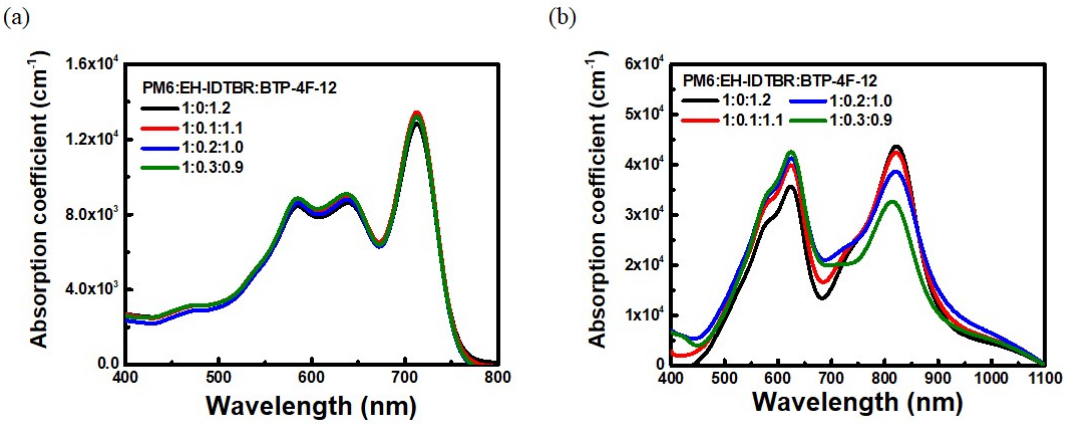

Figure. S1. Absorption coefficient from the UV-vis spectra for the EH-IDTBR-ratio-dependent (a) solution, (b) thin film state of photoactive materials.

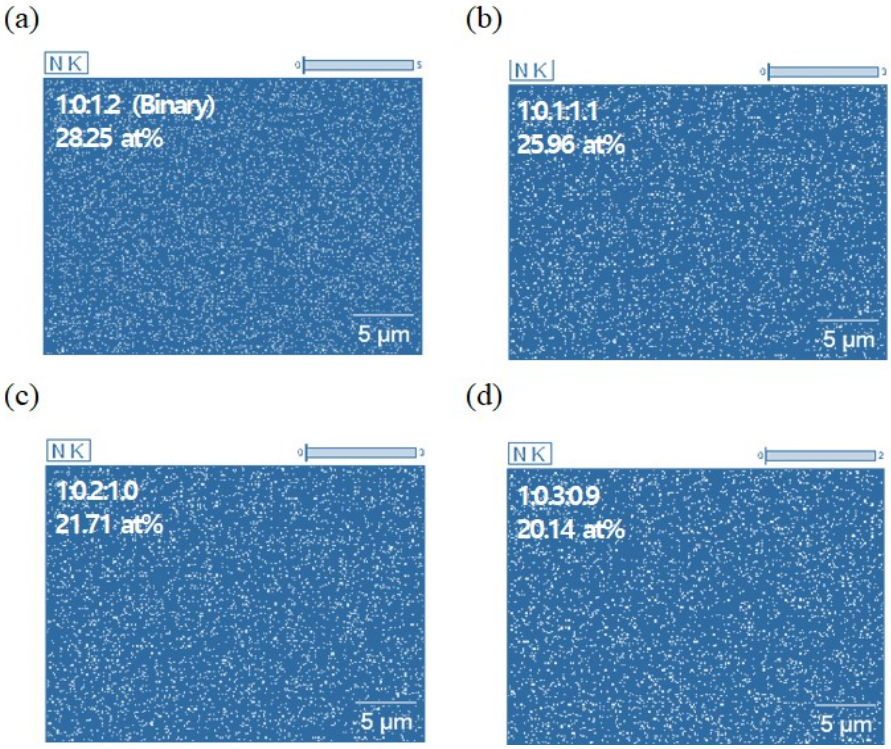

Figure. S2. EDS elemental mapping of N of the binary (a) 0, and (b) 0.1, (c) 0.2 , and (d) 0.3 ratios of EH-IDTBR added ternary photoactive layer.

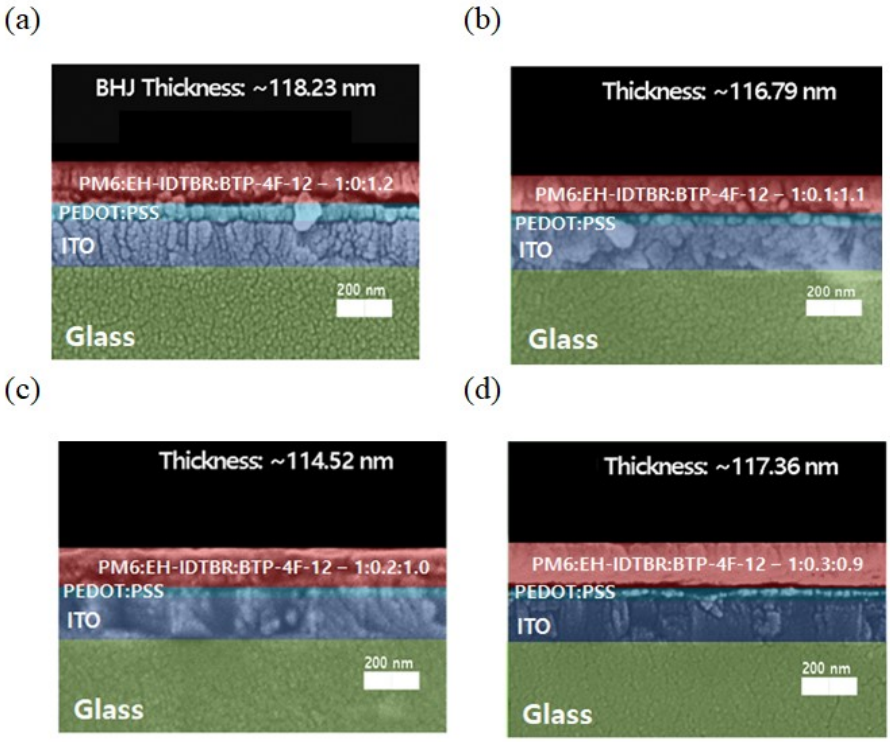

Figure. S3. Thickness of the (a) binary, and (b) 0.1, (c) 0.2, and (d) 0.3 ratios of EH-IDTBR added ternary photoactive layer from the cross-sectional FE-SEM i mages.

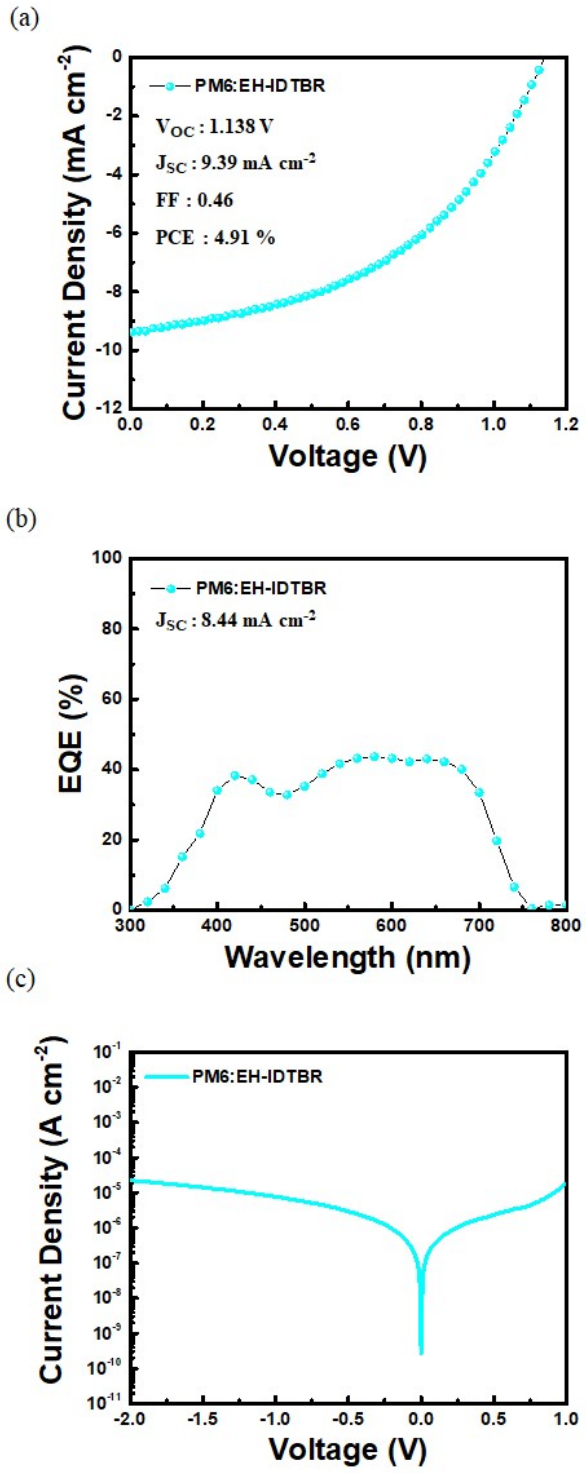

Figure. S4. (a) J-V characteristics of the PM6:EH-IDTBR-based device under AM 1.5G irradiation at 100 mW cm^{-2} and its (b) EQE spectrum. (c) J-V characteristi cs of the PM6:EH-IDTBR devices under dark condition.

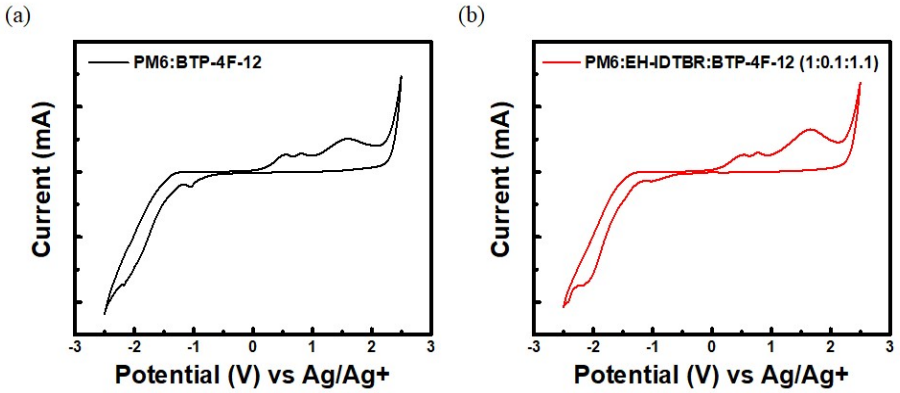

Figure. S5. Cyclic voltammetry curve of the (a) binary (PM6:BTP-4F-12) and (b) optimised ternary (PM6:EH-IDTBR:BTP-4F-12, 1:0.1:1.1) active layers.

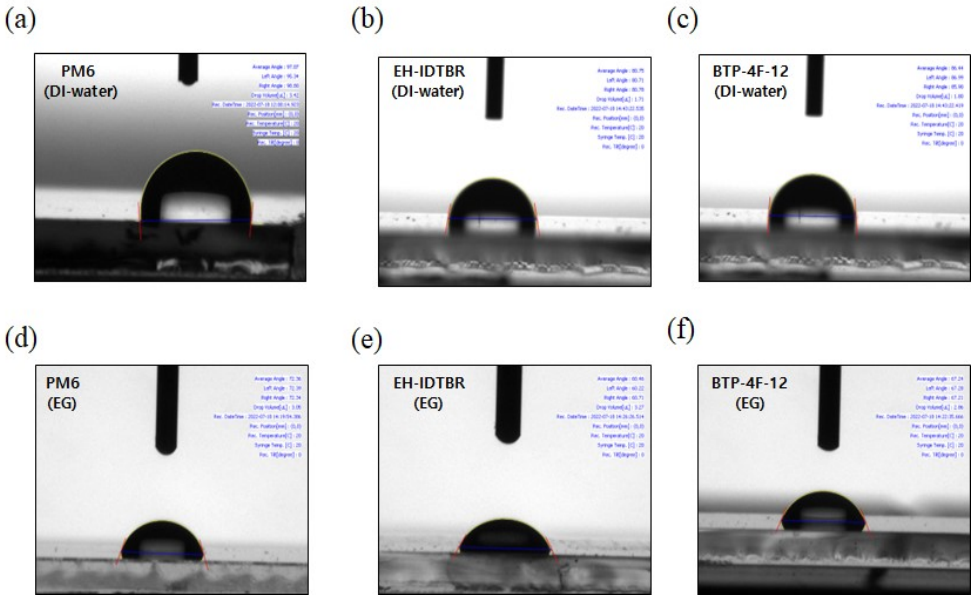

Figure. S6. Contact angle images of the PM6, EH-IDTBR, and BTP-4F-12 with (a–c) deionised water and (d–f) ethylene glycol (EG).

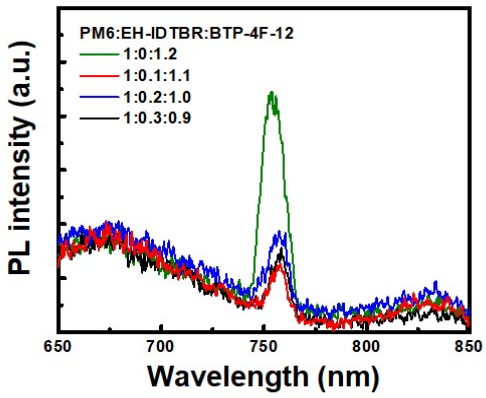

Figure. S7. PL intensities of the EH-IDTBR-ratio-dependent photoactive layer.

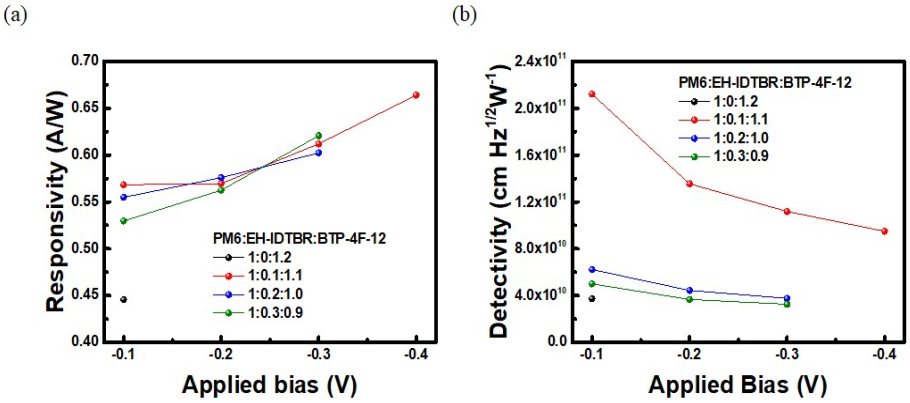

Figure. S8. Applied-bias-dependent device (a) responsivity and (b) detectivity sta bilities of the binary and EH-IDTBR-ratio-dependent ternary devices.

(a)

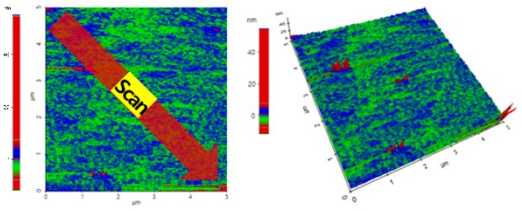

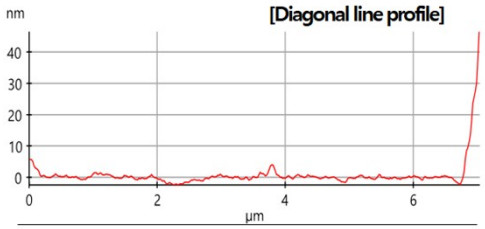

Region	Rpv(nm)	Rq(nm)
Whole	66.437	1.954
Line	48.768	4.556

(b)

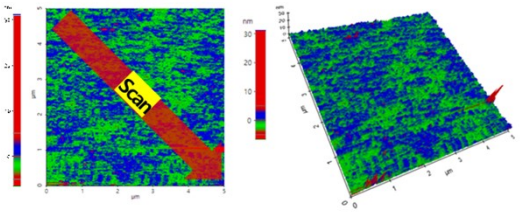

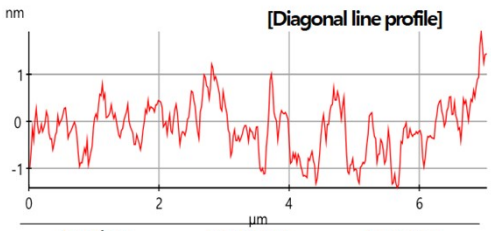

Region	Rpv(nm)	Rq(nm)
Whole	37.766	1.293
Line	3.308	0.567

Figure. S9. Three-dimensional AFM height images of the after applying bias (-0. 1 V) for 600 s for the (a) binary and (b) optimised ternary photoactive layers.

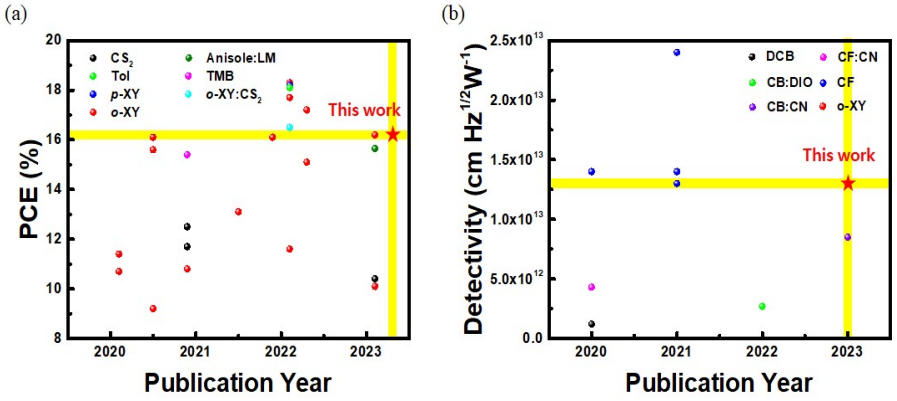

Figure. S10. Recently reported (a) OSCs performances based on non-halogenated solvent (b) self-powered OPDs (> 10^{12} cm $Hz^{1/2}$ W^{-1}).

Table S1. Surface energies of the PM6, EH-IDTBR, BTP-4F-12 layers based on contact angle measurements.

	Contact angle (degree)		$\gamma_{sv}^{dispersive}$	$\gamma_{sv}^{dispersive}$	γ_{sv}
	DI-water (polar)	Ethylene glycol (dispersive)	(mJ m^{-2})	(mJ m^{-2})	(mJ m^{-2})
A (PM6)	97.07	72.36	6.46	5.81	12.27
B (EH-IDTBR)	80.75	60.46	18.41	6.23	24.64
C (BTP-4F-12)	86.44	67.24	14.74	8.60	23.34

Table S2. Calculated charge mobility and trap density from the SCLC plots of t he EH-IDTBR-ratio-dependent active-layer-based devices.

	Mobility ($cm^2 V^{-1}s^{-1}$)		Trap-density (# cm^{-3})	
	Hole-only	Electron-only	Hole-only	Electron-only
1:0:1.2	4.8×10^{-5}	2.7×10^{-5}	1.2×10^{16}	9.7×10^{15}
1:0.1:1.1	3.9×10^{-5}	2.6×10^{-5}	1.0×10^{16}	4.8×10^{15}
1:0.2:1.0	3.5×10^{-5}	2.2×10^{-5}	1.0×10^{16}	5.5×10^{15}
1:0.3:0.9	1.1×10^{-5}	1.1×10^{-4}	9.5×10^{15}	7.6×10^{15}

Table S3. Fitted values for the equivalent circuit from impedance spectroscopy.

	R_{CT} (Ω)	R_{REC} (Ω)
1:0:1.2	16.3	981
1:0.1:1.1	11.4	5822
1:0.2:1.0	11.9	3373
1:0.3:0.9	13.9	2051

Table S4. Recently reported OSCs performances based on non-halogenated solvents.

Solvent	Materials	PCE (%)	Ref.
CS_2	PBDB-T:ITIC	10.4	[1]
CS_2	PM7:IT-4F	11.7	[2]
CS_2	PM7:IT-4Cl	12.5	[2]
TMB	PM6:Y6	15.4	[3]
Tol	PM6:BO-4Cl-Y6-1O	18.1	[4]
Anisole:LM	PBNT-TzTz:Y6-BO	15.7	[5]
p-XY	PM6:BO-4Cl:1O	18.2	[4]
o-XY:CS_2	PM6:Y6	16.5	[6]
o-XY	PM7:IT-4Cl	10.8	[2]
o-XY	PM6:Y6	15.6	[3]
o-XY	PM6:Y6	11.6	[4]
o-XY	PM6:BO-4Cl:Y6-1O	18.3	[4]
o-XY	PM6:BO-4Cl	17.7	[4]
o-XY	PTB7-Th:F10IC2	10.7	[7]
o-XY	PTB7-Th:F10IC2	11.4	[7]
o-XY	PM6:YSe-C6	16.1	[8]
o-XY	PM6:PY2F-T	13.1	[9]
o-XY	PPDT2FBT:$PC_{61}BM$	9.2	[10]
o-XY	PM6:DTY6	16.1	[11]
o-XY	PM6:BTP-eC9	17.2	[12]
o-XY	PM6:Y6	15.1	[12]
o-XY	D18:BTP-eC9	16.2	[13]

o-XY	TPD-3F:IT-4F	10.1	[14]
o-XY	PM6:EH-IDTBR:BTP-4F-12	16.2	This work

Table S5. Recently reported high performance (> 10^{12} cm $Hz^{1/2}$ W^{-1}) self-powered OPDs.

Solvent	Materials	Detectivity (Jones, @ 0 V bias)	Ref.
DCB	P3HT:PTB7	1.2×10^{12} (745 nm)	[15]
CF:CN (1 vol%)	PTB7-Th:W1	4.3×10^{12} (830 nm)	[16]
CF	PolyTPD:SBDTIC	1.4×10^{13} (740 nm)	[17]
CF	PM6:PDTTIC-4F	2.4×10^{13} (920 nm)	[18]
CF	D18:Y6	1.4×10^{13} (805 nm)	[19]
CF	PM6:PDTTIC-4F	1.3×10^{13} (900 nm)	[20]
CB:DIO (0.75 vol%)	PM6:IT-4F	2.7×10^{12} (770 nm)	[21]
CB:CN (0.5 vol%)	PM6:Y6	8.5×10^{12} (840 nm)	[22]
o-XY	PM6:EH-IDTBR:BTP-4F-12	1.3×10^{13} (840 nm)	This work

References

[1] ACS Appl. Energy Mater. 2023, **6**, 3, 1595–1604

[2] Org. Electron., 2020, **85**, 105871

[3] Adv. Mater., 2020, **32**, 2002302

[4] Adv. Funct. Mater., 2022, **32**, 2107827

[5] Mater. Horiz., 2023,**10**, 473-482

[6] Nano Energy, 2022, **91**, 106678

[7] Sol. RRL, 2020, **4**, 2000108

[8] J. Mater. Chem. A, 2021, **9**, 24622—24630

[9] Adv. Funct. Mater., 2021, **31**, 2100791

[10] Sol. RRL, 2021, **5**, 2100213

[11] Joule, 2020, **4**, 2004—2016

[12] Energy Environ. Sci., 2022, **15**, 2130—2138

[13] Adv. Energy Mater. 2023, **13**, 2203465

[14] J. Mater. Chem. A, 2023,**11**, 2419-2430

[15] ACS Appl. Mater. Interfaces 2020, **12**, 11, 13061–5155

[16] ACS Appl. Mater. Interfaces. 2020, **12**, 39515–39523

[17] Adv. Opt. Mater. 2020, **8**, 1902056

[18] J. Am. Chem. Soc. 2021, **143**, 4281–4289

[19] Adv. Funct. Mater. 2021, **22**, 2106326

[20] ACS Materials Lett. 2022, **4**, 882–890

[21] ACS Appl. Electron. Mater. 2022, **4**, 1567–1575

[22] ACS Sustainable Chem. Eng. 2023, **11**, 625–637